Supporting Information for:

Urban NO_x emissions around the world declined faster than anticipated between 2005 and 2019

This PDF file includes:

Exponentially Modified Gaussian (EMG) Function Fit of OMI NO_2 Data Methodology

The original methodology, proposed by Beirle et al. (2011) applied to OMI NO_2 data, involves the fitting of satellite NO_2 line densities to an EMG function. NO_2 line densities are the integral of the NO_2 satellite retrieval perpendicular to the path of the plume; the units are mass per distance. The EMG model is expressed as:

$$TROPOMI\ NO_2\ Line\ Density = \alpha\left[\frac{1}{x_o} exp\left(\frac{\mu}{x_o} + \frac{\sigma^2}{2x_o^2} - \frac{x}{x_o}\right)\Phi\left(\frac{x-\mu}{\sigma} - \frac{\sigma}{x_o}\right)\right] + \beta \quad (2)$$

where α is the total number of NO_2 molecules observed near the hotspot, excluding the effect of background NO_2, β; x_o is the e-folding distance downwind, representing the length scale of the NO_2 decay; μ is the location of the apparent source relative to the city center; σ is the standard deviation of the Gaussian function, representing the Gaussian smoothing length scale; Φ is the cumulative distribution function. Using the 'curvefit' function in IDL, we determine the five unknown parameters: α, x_o, σ, μ, β based on the independent (distance; x) and dependent (TROPOMI NO_2 line density) variables.

Using the mean zonal wind speed, w, of the NO_2 line density domain, the mean effective NO_2 lifetime $\tau_{effective}$ the mean NOx emissions can be calculated from the fitted parameters x_o and α:

$$NO_x\ Emissions = 1.33\left(\frac{\alpha}{\tau_{effective}}\right), \text{ where } \tau_{effective} = \frac{x_o}{w} \quad (3)$$

The factor of 1.33 is the mean column-averaged NO_X / NO_2 ratio and is time-dependent, spatially varying and is primarily a function of the localized j(NO_2) and O_3 concentration. The average NO_X emissions rate and effective photochemical lifetime of NO_2 can be derived from the parameters that describe the best statistical fit. We use a minor update to the Beirle et al. (2011) method by rotating each day's urban NO_2 plume by the mid-afternoon wind direction to force a westerly wind direction; this minor update, originally proposed by Valin et al. (2013), allows for more data, and reduces uncertainties related to the wind direction.

Discussion of Methodological Uncertainties

Tropospheric vertical column amounts in urban areas are underestimated by satellite instruments due to fine spatial heterogeneities of NO_2 pollution and a potential systematic air mass factor bias (Chan et al., 2018; S. Choi et al., 2020; Goldberg et al., 2017; Herman et al., 2019; Ma et al., 2013). This low bias still remains in the NASA version 4.0 product although it is improved from prior algorithm versions (Lamsal et al., 2021). One potential source of the low bias is the use of coarse (1º × 1.25º) a priori vertical NO_2 profiles used in the air mass factor calculation. The result of using a high-resolution model to provide NO_2 vertical shape profiles varies from city to city, but was quantified for a megacity (Seoul, Korea) to be 1.37 using information from the KORUS-AQ field campaign (Goldberg, Saide, Lamsal, De Foy, et al., 2019). To quantify the bias in each city, it would involve vertical NO_2 profile measurements and a high-resolution (~4 km) regional chemical transport model simulation, which are lacking in most urban areas. Because most cities in our analysis are of similar size to Seoul, we uniformly apply this conversion factor, while simultaneously noting its large uncertainty (~30%).

In areas of large anthropogenic aerosol loadings, such as India and central Africa, the aerosol explicit effects on the air mass factor are further biasing the satellite measurement low (Cooper et al., 2019; M. Liu et al., 2019; Vasilkov et al., 2021). Studies have shown that high aerosol loadings generally shift the vertically-resolved instrument sensitivity to higher in the atmosphere, decreasing the instrument sensitivity near the surface (Chimot et al., 2016; Leitão et al., 2010). Instead of applying regional correction factors in areas of high near-surface aerosol loadings, we decide to report the values as is, with the caveat that there is a high likelihood the magnitude of top-down NO_X emissions values in India and central Africa are low, and have larger uncertainties than other urban areas.

The wind speed and direction are also major sources of uncertainty. Errors in the wind direction will lead to an incomplete plume rotation and shorten the effective NO_2 lifetime. Veering of the wind with time will induce a similar artificial shortening of the effective NO_2 lifetime. Wind direction errors are accounted for the statistical fit by the exponential decay fitting parameter. Wind speed errors, however, are not directly accounted for in the statistical fit. In our method, we assume the effective speed of the NO_2 plume is analogous to the 100-m wind speed: a faster or slower speed will cause a larger or smaller inferred emission rate, respectively. Further, errors in the rotation will manifest in the wind speed because an incomplete rotation will yield an

effective horizontal wind speed that is slower than reality. We choose a 100-m wind speed and direction because it is readily available from the ERA5 re-analysis and is a value in-between the surface winds and the mean winds within the boundary layer. A case study performed on Dallas, Texas shows variation of ±25% if using the near surface (-22%) or 500-m wind speed (+18%) in lieu of the 100-m wind speed (Table S1).

The spatial matching between top-down and bottom-up emissions datasets is another large source of uncertainty. The top-down satellite estimate quantifies the emissions of a Gaussian plume with sigma representing its width; the area within ±1-sigma should contain 68% of the signal and 95% of the signal within ±2-sigma. In order to match the top-down estimate with the bottom-up inventory, we need to assume an explicit width of the plume. For our comparison, we assume that at a distance of ±2-sigma, we are capturing the urban area's plume. We use ±2-sigma in lieu of extending to ±3-sigma because emissions at the outskirts of an urban area contribute the background concentration and not the urban plume; including too much of the outer edges of an urban area is not an appropriate comparison. Using distances much less than 2-sigma would likely not capture the full-extent of the urban plume. Most importantly, 2-sigma of the top-down fit varies from city-to-city and year-to-year (smaller for smaller urban plumes), and is accounted for when comparing to the bottom-up inventories. If assuming a 1.5-sigma distance, bottom-up emissions decrease by roughly 30%, and if using a 3-sigma distance, bottom-up emissions increase by roughly 30% (Figure S4).

We calculate the early afternoon adjustment factor based on temporal emission patterns described in Denier van der Gon et al. (2011). We were able to calculate that emissions at 13:00 local time are 1.30 times larger than the 24-hour average NOx emissions rate, yielding a correction factor of 0.77. This correction factor was calculated assuming the following NOx emissions sector allocation in an urban area: 50% mobile sources, 25% industrial combustion, 10% residential combustion, 10% power generation, 5% other. This is also identical to correction factor calculated in Boersma et al. (2008). In a hypothetical mobile-centric city (70% mobile emissions), the value is 0.74, and for an industrial-centric city (40% industrial emissions), the value is 0.79. On a continental scale, Denier van der Gon et al. (2011) report the ratio to be 0.81, but this is not correct for cities, since power generation is often located outside of city centers and is the cause for the higher ratio. A 20% uncertainty in the mobile source allocation, the most

variable value between cities, would cause the ratio to vary between 0.69 and 0.86, yielding a total uncertainty of 10%.

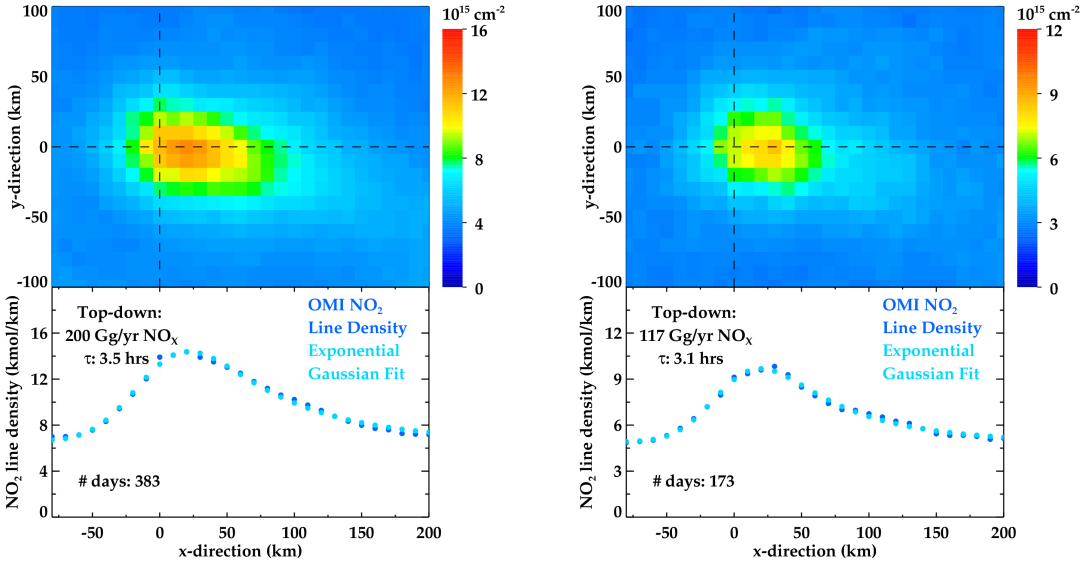

Figure S1. Illustrative example of the top-down method applied to Paris for the (left) 2005-207 period and (right) 2017 – 2019 period

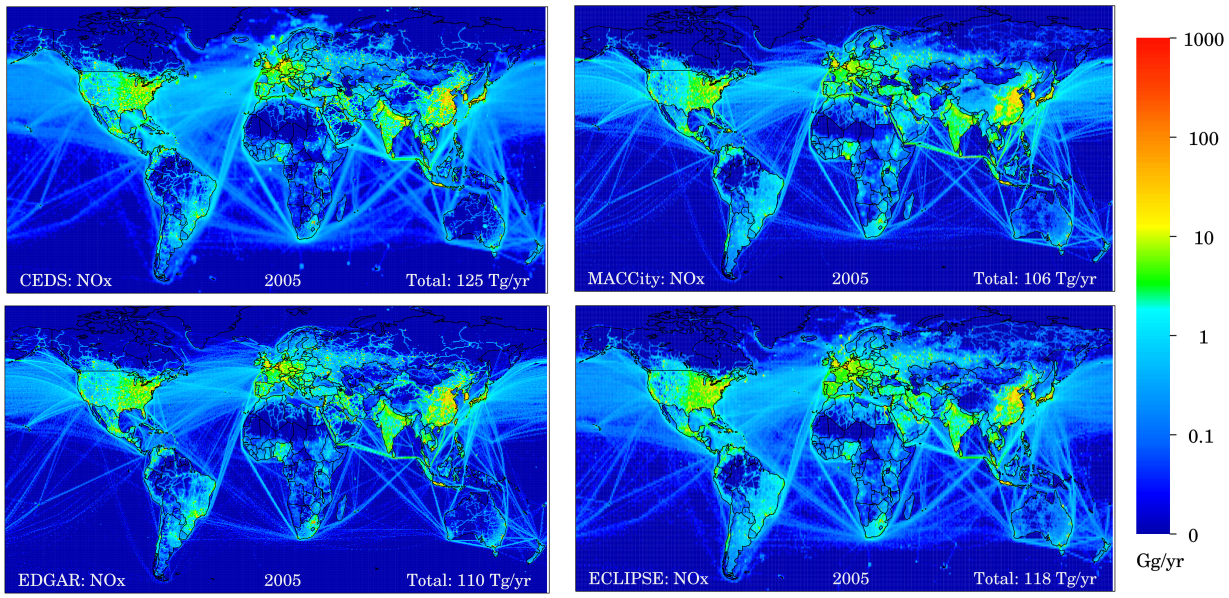

Figure S2. Spatial representation of all four NOx emission inventories in 2005 (CEDS, MACCity, EDGAR, ECLIPSE) in units of Gg/yr NO_2 per grid cell

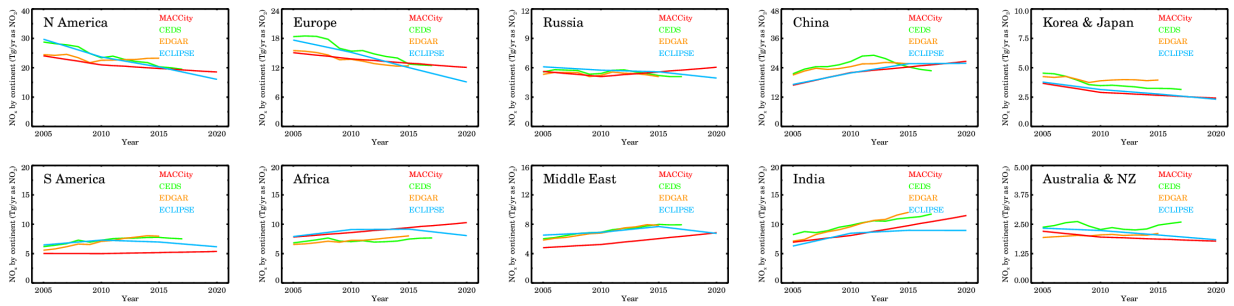

Figure S3. Annual trends of the four NOx emission inventories (CEDS, ECLIPSE, EDGAR, and MACCity) in units of Tg/yr across all grid cells

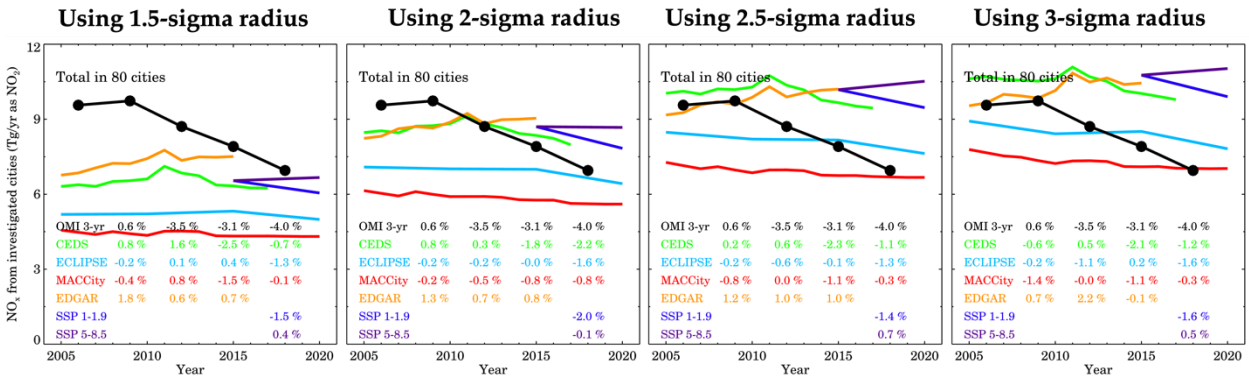

Figure S4. Aggregating the bottom-up inventories to various radii from the city center, and comparison to the top-down estimates, which are constant in each scenario

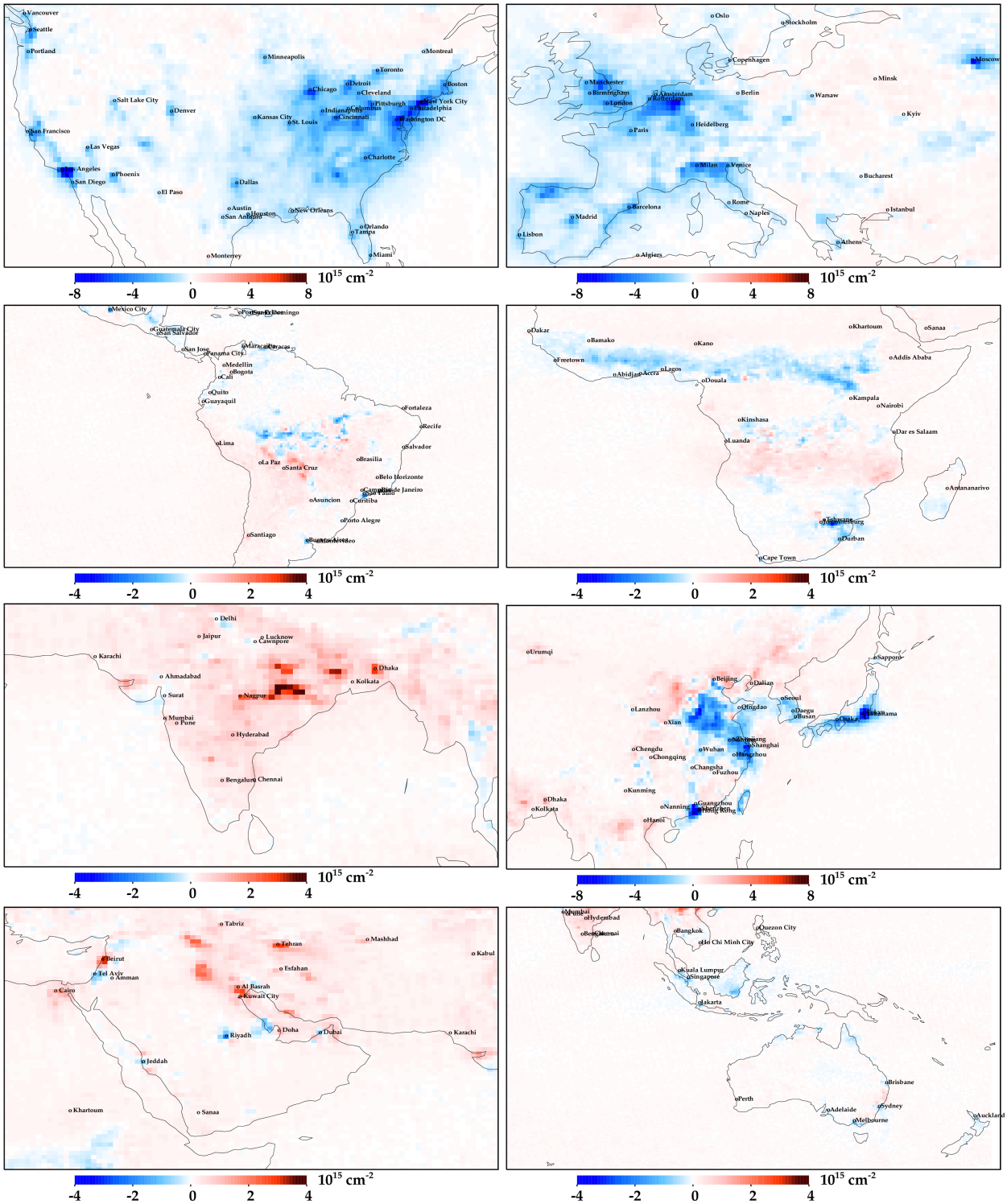

Figure S5. Regional trends in OMI tropospheric vertical column NO_2 between 2005 and 2019 annual averages. Spatial resolution of the annual data is 0.1° × 0.1°, and is aggregated to 0.5° × 0.5° for clarity.

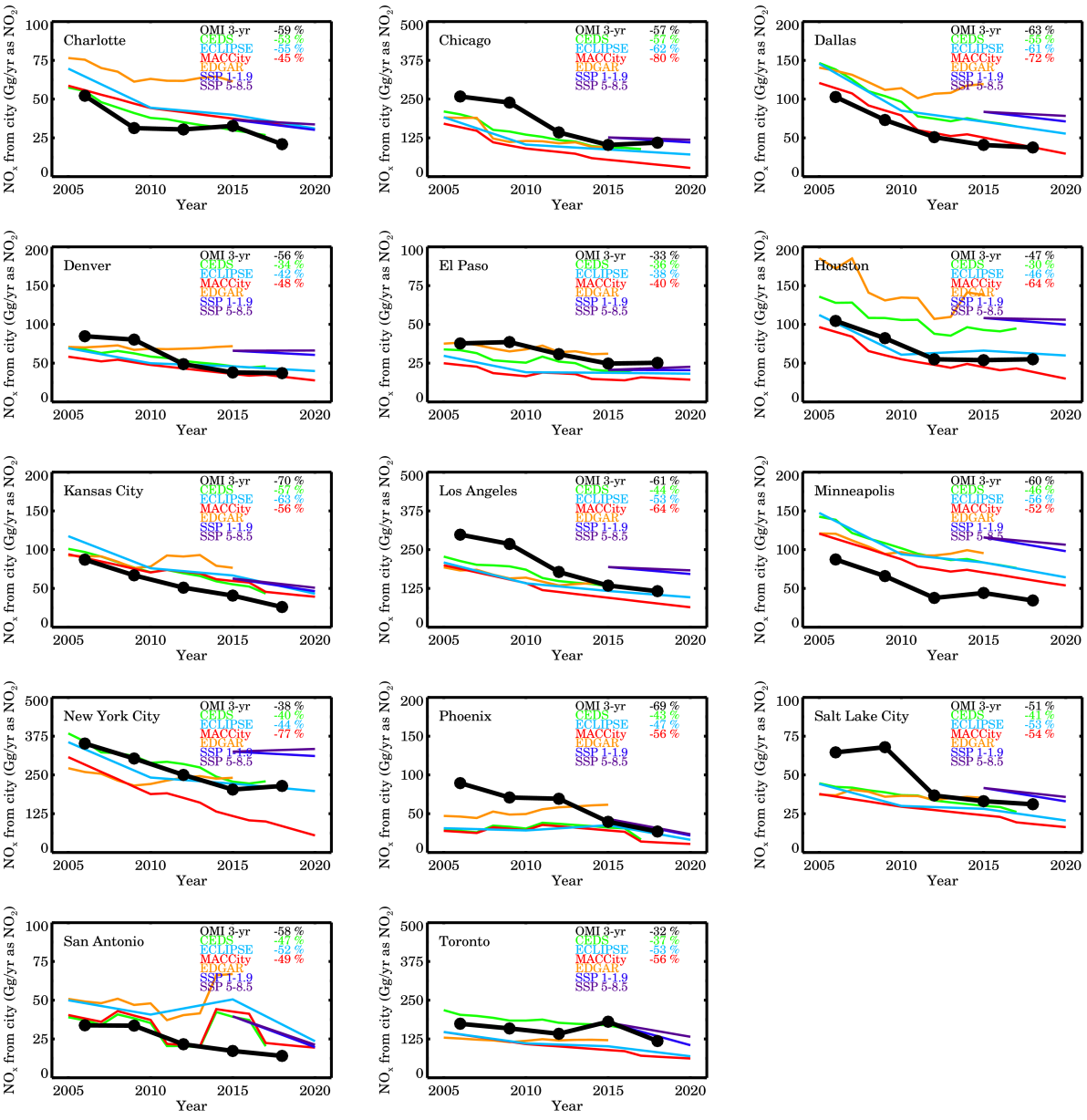

Figure S6. Top-down vs. Bottom-up NO_X comparison in US & Canadian urban areas

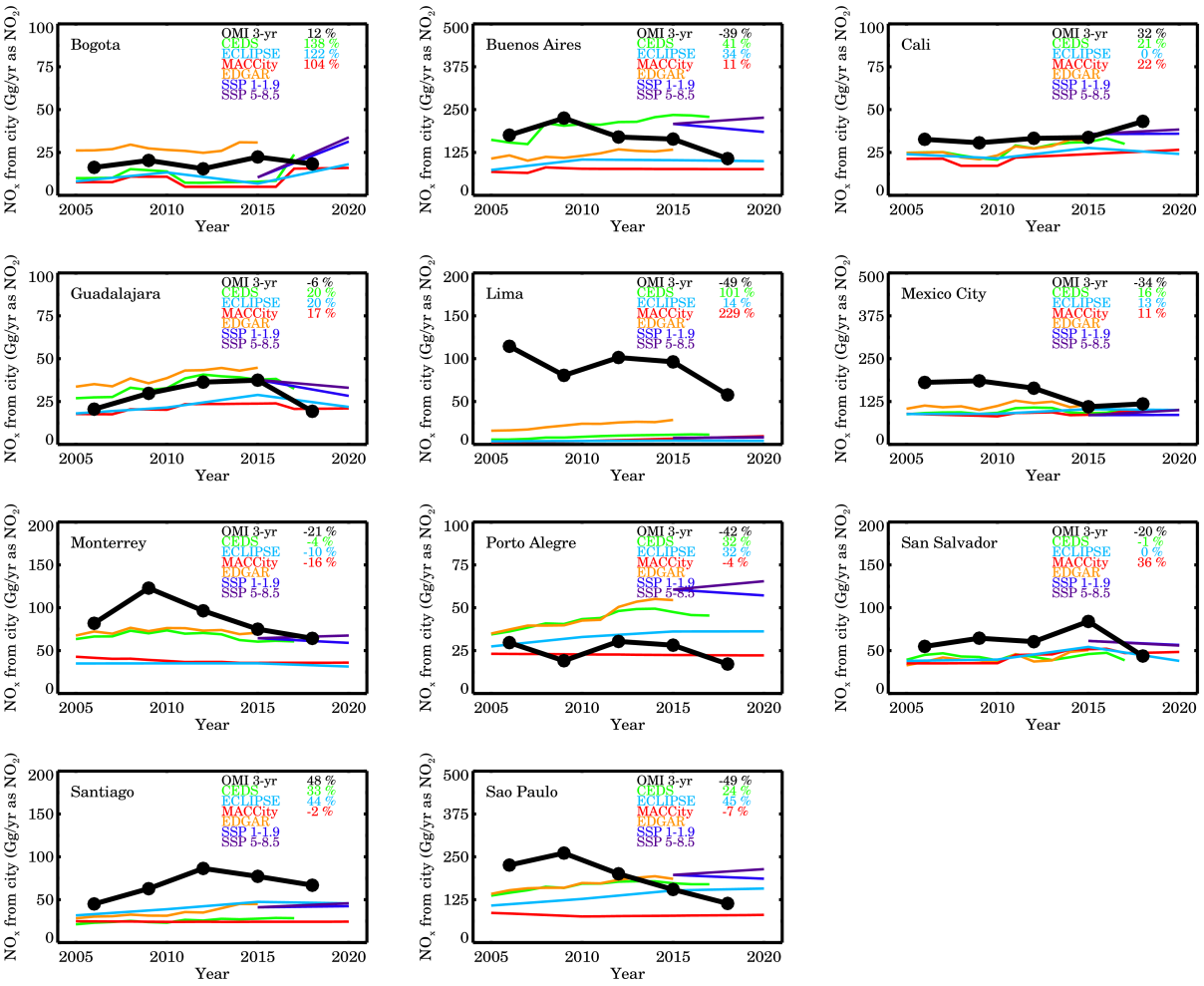

Figure S7. Top-down vs. Bottom-up NO_X comparison in Latin American urban areas

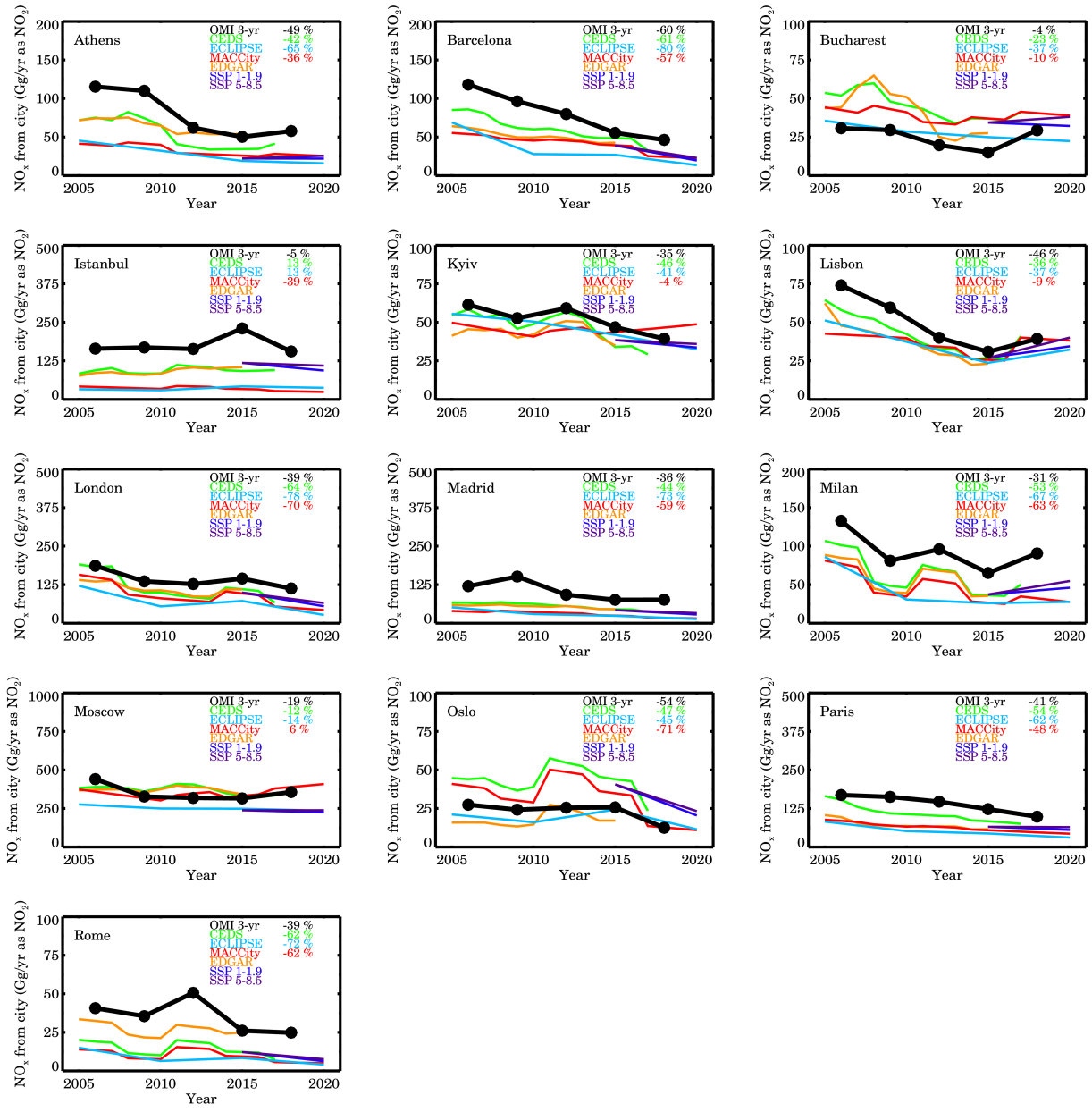

Figure S8. Top-down vs. Bottom-up NO_X comparison in European urban areas

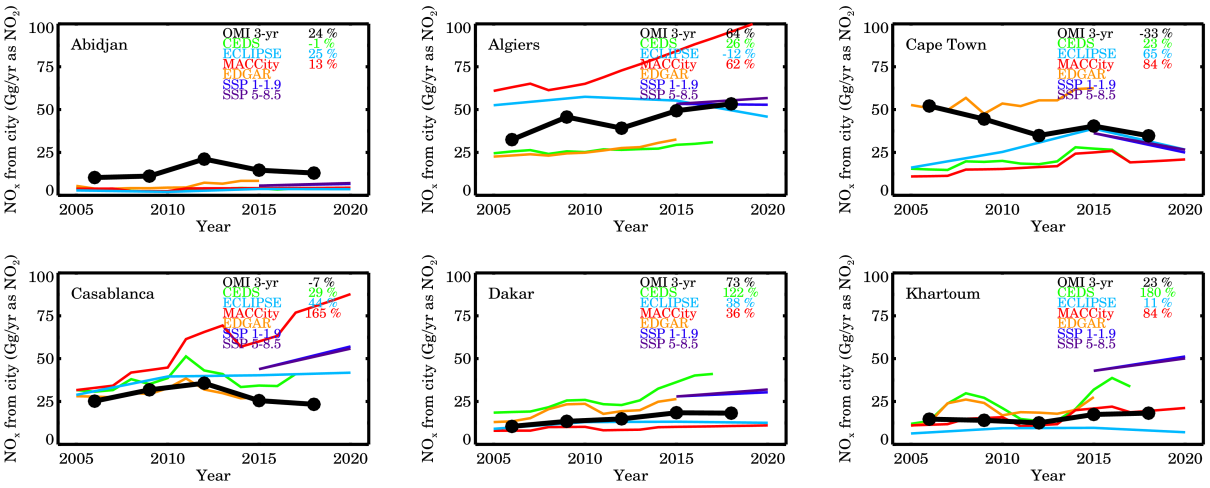

Figure S9. Top-down vs. Bottom-up NO_X comparison in African urban areas

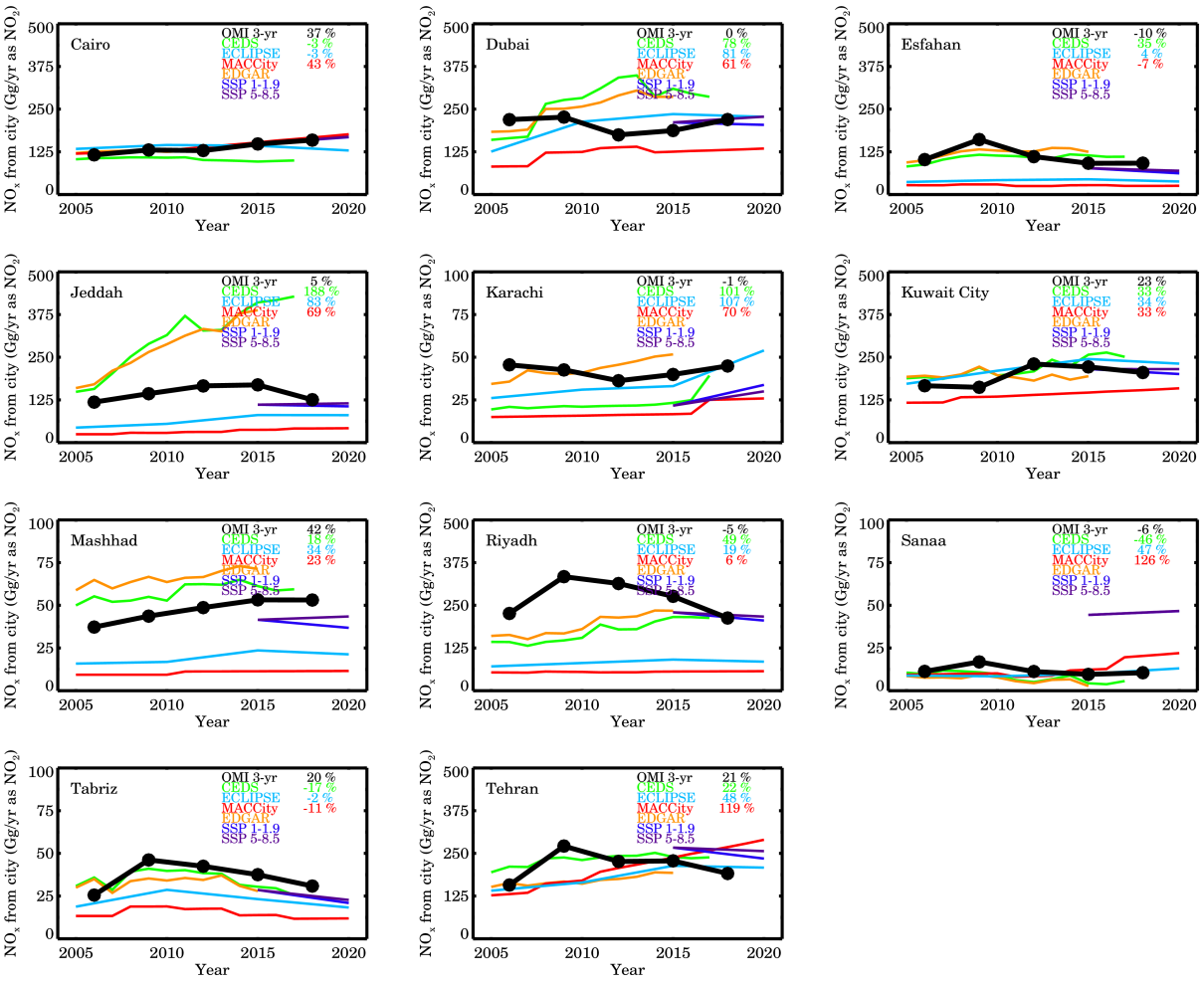

Figure S10. Top-down vs. Bottom-up NO_X comparison in Middle Eastern urban areas

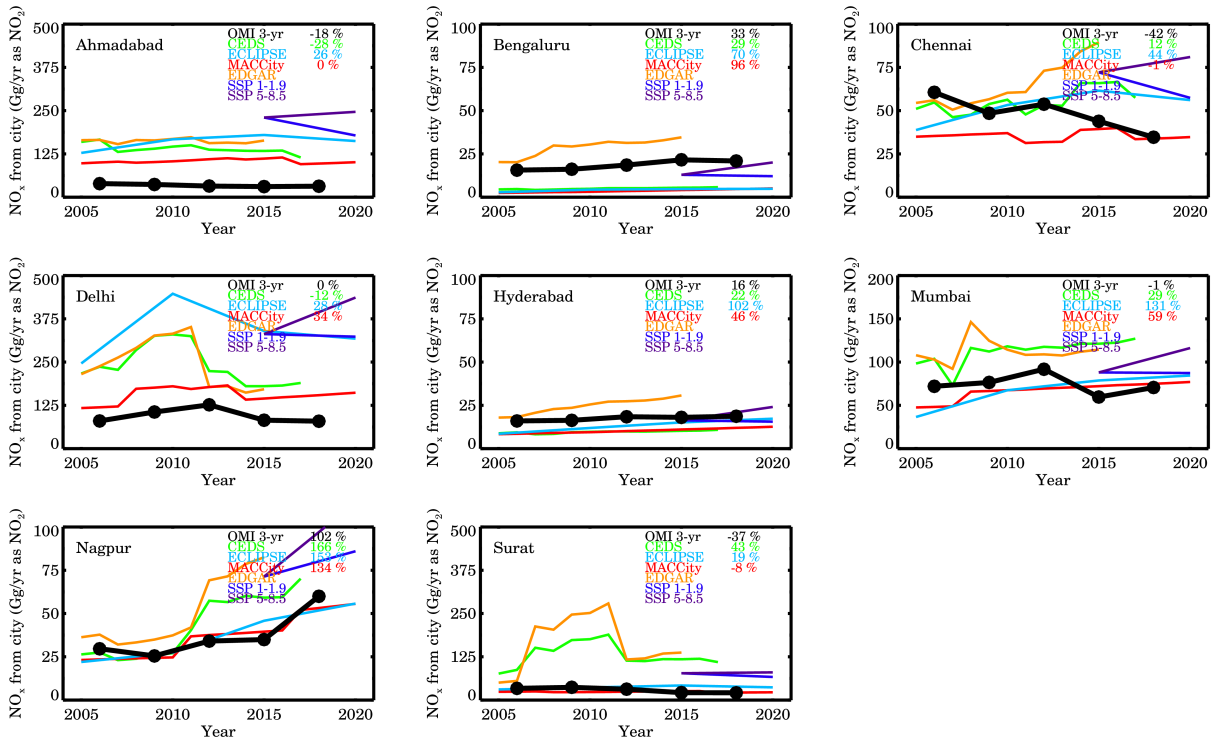

Figure S11. Top-down vs. Bottom-up NO_X comparison in Indian urban areas

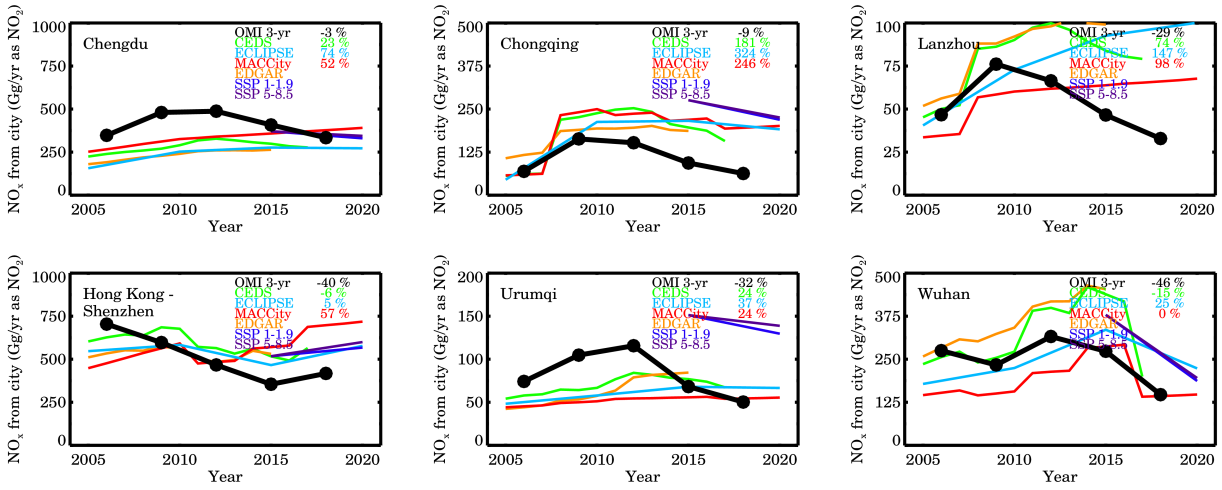

Figure S12. Top-down vs. Bottom-up NO_X comparison in Chinese urban areas

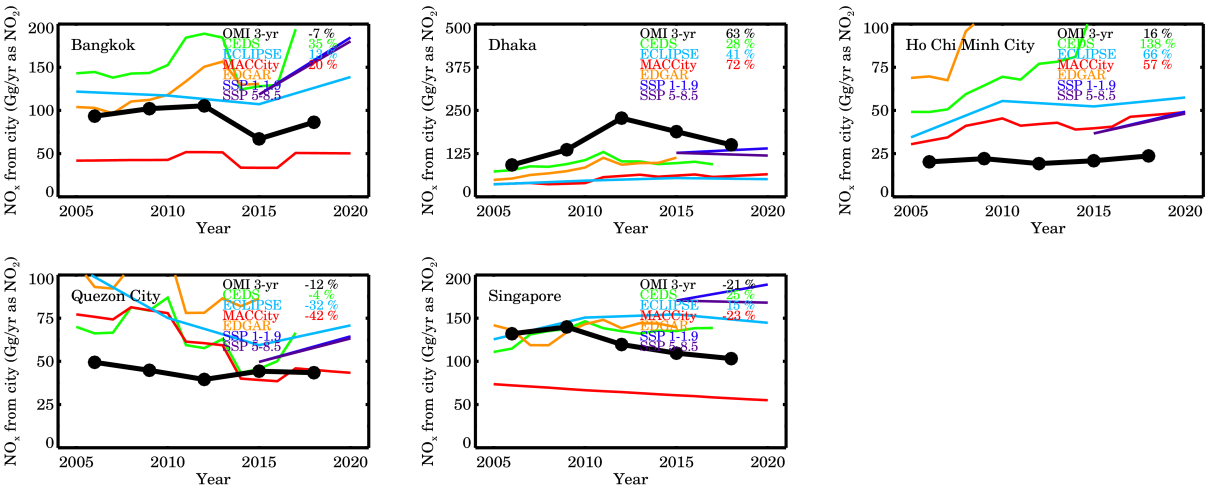

Figure S13. Top-down vs. Bottom-up NO_X comparison in Southeastern Asian urban areas

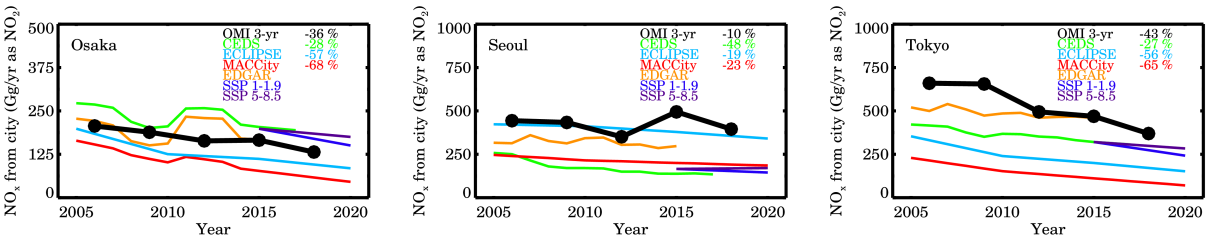

Figure S14. Top-down vs. Bottom-up NO_X comparison in Korean & Japanese urban areas

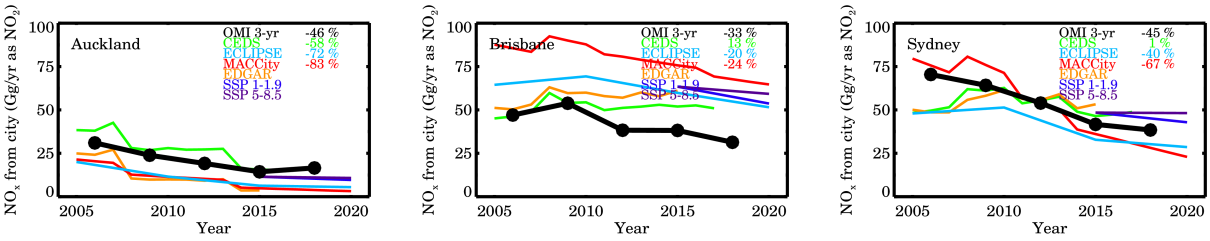

Figure S15. Top-down vs. Bottom-up NO_X comparison in Australasian urban areas

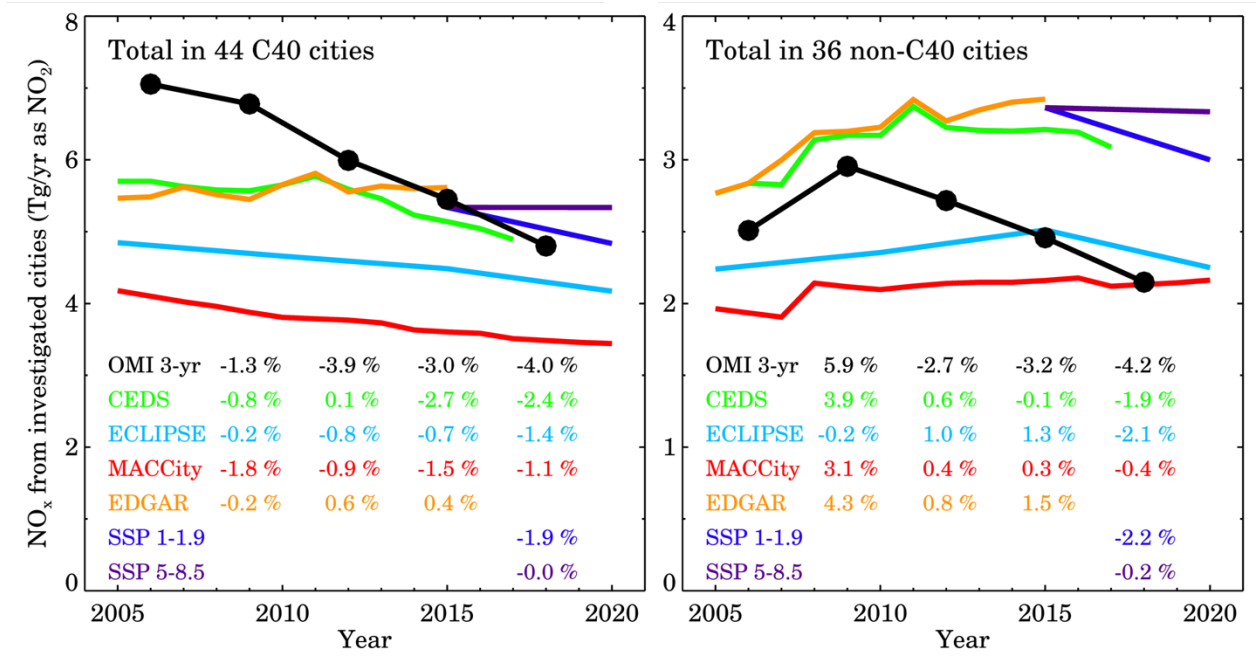

Figure S16. Top-down vs. Bottom-up NO_X comparison C40 and non-C40 urban areas

Table S1. Top-down method applied to Dallas-Fort Worth as a case study in 2019, using winds at three different heights: 100-m, surface, and 500-m

Wind fields	**NOx Emission rate**
100-m winds at 16-19Z	45 Gg/yr
Surface winds at 16-19Z	35 Gg/yr
500-m winds at 16-19Z	53 Gg/yr

Table S2. Relative NOx emission temporal patterns at the local time of day, calculated using temporal disaggregation factors provided in Denier van der Gon et al. (2011). Factors at 13:00 local time are highlighted due to coincident OMI measurement at the time. A typical urban area is calculated by assuming the following sector allocation: 50% mobile sources, 25% industrial combustion, 10% residential combustion, 10% power generation, 5% other/waste treatment. High-mobile assumes 70% mobile emissions; High-industrial assumes 40% industrial emissions.

Local Time of Day	**0**	**1**	**2**	**3**	**4**	**5**	**6**	**7**	**8**	**9**	**10**	**11**	**12**	**13**	**14**	**15**	**16**	**17**	**18**	**19**	**20**	**21**	**22**	**23**
Typical Urban area	0.45	0.39	0.38	0.39	0.43	0.53	0.95	1.50	1.55	1.34	1.25	1.21	1.24	**1.30**	1.30	1.35	1.54	1.56	1.29	1.06	0.87	0.80	0.75	0.59
High-mobile Urban	0.35	0.28	0.26	0.26	0.30	0.41	0.91	1.63	1.66	1.36	1.24	1.20	1.27	**1.35**	1.36	1.44	1.74	1.77	1.37	1.05	0.82	0.72	0.69	0.54
High-industrial Urban	0.53	0.49	0.49	0.50	0.54	0.64	0.97	1.39	1.44	1.31	1.25	1.23	1.22	**1.27**	1.27	1.28	1.40	1.40	1.20	1.04	0.89	0.83	0.77	0.63

Table S3. 2-sigma radii (km) for each city and year, as fitted by the EMG plume fit

City	2006	2009	2012	2015	2018
Abidjan	19	17	21	18	18
Ahmadabad	77	83	68	63	51
Algiers	49	47	43	46	44
Athens	38	43	37	36	38
Auckland	50	34	36	24	27
Bangkok	29	32	36	25	33
Barcelona	43	39	46	38	30
Bengaluru	14	13	13	14	16
Bogota	21	26	17	16	32
Brisbane	57	71	66	67	62
Bucharest	57	82	57	64	74
Buenos Aires	34	41	40	40	39
Cairo	90	98	108	110	108
Cape Town	29	37	34	47	33
Casablanca	49	57	67	53	60
Charlotte	51	49	52	78	52
Chengdu	75	111	92	80	82
Chennai	32	28	27	31	26
Chicago	48	42	38	34	37
Chongqing	32	65	62	57	50
Dakar	27	33	25	32	30
Dallas	64	61	49	55	55
Delhi	47	64	60	44	46
Denver	46	52	48	52	55
Dhaka	54	52	59	56	49
Dubai	42	59	63	54	57

El Paso	41	35	42	36	39
Esfahan	46	48	42	43	42
Guadalajara	34	38	47	45	38
Ho Chi Minh City	39	47	42	36	38
Hong Kong	63	63	52	56	62
Houston	38	35	36	41	44
Istanbul	51	50	60	55	50
Jeddah	44	48	57	63	68
Kansas City	79	70	77	72	58
Karachi	21	21	19	21	24
Khartoum	42	44	33	43	41
Kuala Lumpur	30	27	27	32	30
Kuwait City	54	70	91	86	85
Kyiv	55	54	65	50	51
Lanzhou	36	50	48	49	51
Lima	22	21	22	22	22
Lisbon	52	50	45	37	53
London	50	42	40	53	42
Los Angeles	49	48	47	45	47
Madrid	37	41	38	35	31
Mashhad	33	33	41	40	40
Mexico City	40	38	43	42	45
Milan	48	36	51	37	45
Minneapolis	69	68	63	87	92
Monterrey	50	53	49	45	43
Moscow	51	51	59	47	55
Mumbai	32	35	37	36	34
Nagpur	32	29	42	39	55

Nanjing	42	48	57	65	45
New York City	50	49	53	50	57
Osaka	58	54	69	61	60
Oslo	50	45	69	59	36
Paris	41	36	39	35	36
Phoenix	30	36	39	38	30
Porto Alegre	95	101	112	109	107
Quezon City	49	53	47	36	38
Riyadh	45	56	52	54	53
Rome	25	21	30	23	22
Salt Lake City	48	49	48	52	43
San Antonio	40	43	37	60	42
San Salvador	56	53	65	71	82
Sanaa	32	30	27	31	47
Santiago	29	28	29	31	32
Sao Paulo	43	47	44	45	47
Seoul	43	43	43	44	46
Singapore	25	27	27	25	26
Surat	39	37	36	35	29
Sydney	34	41	33	31	29
Tabriz	37	52	44	34	30
Tehran	37	42	47	44	43
Tokyo	57	57	57	56	54
Toronto	48	48	52	52	39
Urumqi	41	47	50	48	45
Wuhan	46	40	51	58	37

Table S4. Effective NO_2 lifetime for each city and year, as fitted by the EMG plume fit and ERA5 wind speeds

City	2006	2009	2012	2015	2018
Abidjan	1.1	1.1	0.7	1.1	1.3
Ahmadabad	4.1	5.0	4.9	4.4	5.0
Algiers	3.2	2.3	3.2	2.8	2.8
Athens	2.1	1.8	1.9	2.3	2.1
Auckland	3.9	3.0	5.4	6.0	6.6
Bangkok	2.8	3.0	3.3	4.9	3.6
Barcelona	3.8	3.0	3.3	4.0	4.2
Bengaluru	0.8	1.4	1.2	1.2	1.4
Bogota	3.4	2.8	5.4	3.6	3.7
Brisbane	3.2	2.9	3.4	3.3	3.9
Bucharest	2.3	3.3	2.8	3.8	3.0
Buenos Aires	2.5	1.7	2.3	2.4	3.0
Cairo	3.6	4.2	4.9	4.3	4.1
Cape Town	2.5	2.3	2.6	2.8	2.7
Casablanca	3.1	2.5	3.0	3.9	4.0
Charlotte	3.9	3.4	2.5	3.4	3.0
Chengdu	1.5	1.7	1.8	1.7	1.9
Chennai	1.4	2.1	1.9	3.0	4.0
Chicago	5.0	2.2	2.9	4.3	3.7
Chongqing	5.8	3.8	4.5	4.6	4.7
Dakar	3.1	2.1	2.9	2.9	2.3
Dallas	4.7	3.2	3.2	5.6	5.2
Delhi	5.1	4.7	3.6	4.6	4.7
Denver	3.9	2.8	4.6	5.1	5.0
Dhaka	2.6	2.2	1.7	2.5	3.4
Dubai	3.0	3.3	3.6	3.6	3.5

El Paso	3.1	2.1	2.6	2.7	2.4
Esfahan	2.5	1.9	2.9	3.1	3.1
Guadalajara	4.5	2.9	2.9	2.2	4.2
Ho Chi Minh City	4.6	4.6	5.9	5.2	5.2
Hong Kong	3.7	3.8	3.3	2.3	2.0
Houston	4.0	2.8	4.0	4.4	4.4
Istanbul	2.6	2.1	2.4	1.6	2.5
Jeddah	3.3	3.2	3.2	3.6	4.0
Kansas City	4.5	2.9	2.8	3.8	4.0
Karachi	3.6	4.1	5.1	6.3	6.9
Khartoum	1.8	2.0	2.2	1.8	2.4
Kuala Lumpur	2.1	2.2	3.4	2.6	3.3
Kuwait City	4.2	3.7	3.1	3.5	3.6
Kyiv	3.0	2.7	2.5	3.0	3.4
Lanzhou	4.8	3.9	4.8	5.1	5.8
Lima	0.7	1.3	1.4	1.5	2.4
Lisbon	3.6	2.3	2.8	2.4	2.8
London	5.6	3.9	5.1	5.1	4.6
Los Angeles	3.5	2.9	3.6	3.6	3.6
Madrid	3.8	2.2	2.7	3.0	2.7
Mashhad	4.0	3.5	3.3	3.6	3.9
Mexico City	3.0	3.0	3.7	4.5	3.8
Milan	5.6	5.9	6.3	6.2	4.3
Minneapolis	5.0	3.1	4.8	3.3	4.3
Monterrey	2.5	1.7	2.1	2.6	3.1
Moscow	3.8	3.2	2.7	3.5	2.6
Mumbai	1.4	1.4	1.2	1.8	1.6

Nagpur	2.7	3.2	2.4	3.2	3.3
Nanjing	3.4	2.1	3.9	1.8	4.5
New York City	3.8	2.9	3.1	3.6	2.5
Osaka	3.2	3.1	3.3	3.1	3.3
Oslo	4.4	3.7	4.7	3.3	7.9
Paris	3.5	2.0	2.6	3.0	3.1
Phoenix	3.3	2.9	2.5	3.6	4.3
Porto Alegre	2.6	5.3	3.2	2.8	5.4
Quezon City	2.6	2.4	2.8	2.8	2.8
Riyadh	2.8	1.9	2.1	2.8	2.8
Rome	2.8	2.6	1.5	2.8	2.7
Salt Lake City	3.9	2.1	4.1	4.5	4.3
San Antonio	2.6	1.8	2.4	3.9	3.3
San Salvador	0.8	0.7	0.9	0.7	0.9
Sanaa	5.7	4.8	4.8	6.0	5.5
Santiago	4.8	3.5	2.7	3.2	3.9
Sao Paulo	2.4	2.1	2.4	2.8	3.5
Seoul	3.5	3.2	4.7	3.0	3.6
Singapore	2.1	1.8	2.3	2.4	2.4
Surat	2.5	2.1	3.0	4.8	7.0
Sydney	4.3	5.2	4.1	5.4	6.1
Tabriz	2.6	2.0	1.9	1.9	2.7
Tehran	3.1	2.1	3.2	3.1	3.8
Tokyo	2.7	2.2	2.6	2.6	2.7
Toronto	3.2	2.6	2.2	1.7	2.3
Urumqi	3.4	2.8	4.0	5.2	4.8
Wuhan	2.3	2.1	2.4	2.5	3.3